Reconstruction of Object-Specific Attenuation Map for Quantitative SPECT[1)]

Zhengrong Liang and Jinghan Ye
Department of Radiology, State University of New York
Stony Brook, NY 11794

Abstract

A method to improve the reconstruction of object-specific attenuation maps for accurate quantification of single-photon emission computed tomography (SPECT) was studied. This method aims to (1) utilize the *a priori* known attenuation coefficients and (2) compensate for the fan-beam truncation of transmission scans in reconstructing the attenuation map. An external radioactive line source was simulated to generate the fan-beam transmission data through a thorax phantom using a single detector of three-headed SPECT configuration. More than half of the 120 projections distributed evenly over 360 degrees were truncated. The thorax phantom had a size of 128^2 array. Emission data was computer synthesized, following the transmission simulation, using two parallel-beam collimated detectors of the SPECT configuration. The simulated emission data was attenuated by the thorax phantom. The transmission data was reconstructed by an iterative maximum *a posteriori* probability algorithm which simultaneously segments the reconstructed attenuation map with the *a priori* known attenuation coefficients of bone, lung, soft tissues, and air. The truncation was compensated in the forward projection by estimating the truncated data. The continuity of the estimated data to the simulated data was considered in the backprojection. The truncation-compensated and segmented attenuation map was used to reconstruct the emission data. Significant improvement (> 5%) in quantification of SPECT was achieved, as compared to the reconstruction using the truncated attenuation map.

I. INTRODUCTION

Quantitative reconstruction for single-photon emission computed tomography (SPECT) has motivated a great research interest in recent years [1-10]. The quantification requires essentially (i) compensation for the deterministic deficiencies (such as photon attenuation, scatter, and depth-dependent detector response) and (ii) suppression of the random inconsistancies (for example, the Poisson noise of photon detection). Other detector-related deficiencies (such as deadtime, mis-calibration, etc), isotope-related effects (such as decay, biological variation, etc), and patient-related inconsistancies (for example, motion, organ dynamics, etc) are either less significant or beyond the scope of this work and so will not be considered.

1) This work was supported by Grant #HL44194, awarded by the National Heart, Lung, and Blood Institute.

0-7803-1487-5/94$04.00©1994IEEE

The determinstic deficiencies are usually compensated by modeling the projection-transform function $\{R_{ij}\}$ [11]:

$$Y_i = \sum_j R_{ij} O_j , \quad i=1,2,3,...,I , \quad j=1,2,3,...,J \qquad (1)$$

where Y_i is the measured datum at detector position i, O_j the image intensity of voxel j, I the number of data elements, and J the number of voxels. The random inconsistancies can be minimized by either low-pass filtering of the measured data [12], or *a priori* constraints on the reconstruction [13]. The accuracy and efficiency are the major objectives for developing quantitative SPECT reconstruction algorithms for clinical applications.

Recently great progress has been made towards these objectives [1-4,14-16]. For example, with currently available HP/730 desktop computer, a quantitative reconstruction of 128^3 image size from cone-beam collimated SPECT can be obtained within 30 minutes [17]. Figure 1 shows a slice of the three-dimensional (3D) reconstruction using an iterative filtered backprojection (FBP) algorithm [1]. In implementing the efficient algorithms [1-4] for clinical studies, the quantitative reconstruction requires (i) the system-specific detector-response kernel, (ii) the scatter component, and (iii) the object-specific attenuation map.

The system-specific detector-response kernel can be measured using a point source at different depths from the collimator in air and/or water. The scatter component can be either measured using dual or triple photo-peak energy windows [18,19], or computed based on the Klein-Nishina formula using the object-specific attenuation map [11]. There have been a great effort devoted previously to reconstruct the object-specific attenuation map [20-25].

It is obvious that the integration of a currently available X-ray computed tomography (CT) scanner with a SPECT system is the solution for reconstructing the attenuation map [22]. The limitations of the integration are (i) the complexity of hardware design and (ii) the cost. If the CT transmission scan and the SPECT emission acquisition are performed separately by a CT scanner and a SPECT system, image registration becomes an obstacle for the attenuation compensation in the SPECT reconstruction. Because of the limitations and the above mentioned obstacle, alternative approaches may be more practical. The approach using an external radioactive point source has the difficulty in reducing the truncation of cone-beam collimation along the axis of detector rotation [23]. The limitation of using an external flat source is mainly due to the high radiation and the difficulty of source collimation [24]. The approach using an external line source has shown very encouraging results [25,26]. However, the trun-

cation of fan-beam collimation remains an unsolved problem.

The goal of this work is to investigate a quantitative method which uses a currently available three-headed SPECT system combining with an external radioactive line source for quantitative reconstruction of emission data. The major effort will be devoted to compensate for the truncation effect associated with the fan-beam collimation.

II. METHOD

The hardware configuration of the quantitative method is shown by Fig.2. An external line source is mounted between two detectors with parallel-hole collimators and faces to a fan-beam collimated detector. The transmission and emission scans are performed either sequentially (in which the line source is a same radiopharmceutical as that administered into the body) or simultaneously (in which the line source is a different radiopharmceutical as that administered into the body).

The software of the quantitative method consists of two reconstruction algorithms. One is a maximum *a posteriori* probability (MAP) reconstruction of the transmission data:

$$\mu_k^{(n+1)} = \bar{\mu}_k^{(n)} \frac{\sum_i T_{ik}}{\sum_i T_{ik} \left[\left(\sum_j T_{ij} \mu_j^{(n)} \right) / X_i \right]} \qquad (2)$$

where X_i is the transmission datum measured at detector position i, μ_j the attenuation coefficient of voxel j, T_{ij} the projection-transform matrix for the fan-beam geometry, and n the iterative index. The penalty term $\bar{\mu}_k^{(n)} = \mu_k^{(n)} (1 - M_k)$ and M_k is the nomalized partial differentiation of the log *a priori* probability considering the known attenuation coefficients of bone, lungs, soft tissues, and air [27,28]. The other is a MAP reconstruction of the emission scans:

$$O_k^{(n+1)} = \bar{O}_k^{(n)} \frac{\sum_i R_{ik} \left[Y_i / \sum_j R_{ij} O_j^{(n)} \right]}{\sum_i R_{ik}} \qquad (3)$$

where $\bar{O}_k = O_k^{(n)} / (1 + N_k)$ and N_k is the nomalized partial differentiation of the log *a priori* probability reflecting the correlations over the neighborhood of voxel k [1,5].

The main obstacle in implementing the reconstruction algorithms is the truncation problem associated with the fan-beam collimation of the transmission scans. The compensation for the truncation effect is described as follows.

As shown in Fig.3, the truncated areas a and b in the projection at angle 1 are sampled by the projection at angle 2. In a similar manner, the truncated parts c and d in the projection at angle 2 are sampled by the projection at angle 1. It is clear that the truncation causes only a partial-information loss. This is different from the cone-beam collimation where the truncation along the axis of rotation causes a complete-information loss. This observation suggests to estimate the missed data by reprojecting the previously reconstructed source iteratively. Since the reprojected data from areas a and b at projection angle 2 will be corrected by the measured data at that angle, a sequential correction of projection/backprojection at each angle would be optimal.

When the reprojection is computed, a continuity constraint is necessary to match the reprojection to the measured projection before backprojection. As shown in Fig.4, the solid line represents the measured-data profile at a projection angle with truncations at positions g and h. The dotted lines are assumed to be parts of the reprojected data from the truncated areas (the center part is omitted). The continuity constraint requires the dotted lines match the solid line at the positions g and h, respectively.

It can be questioned immediately that how far can the dotted lines go away from the positions g and h, respectively, before they drop to zero? The initial constraint on the drop-off is the scan orbit recorded during detector rotation. Although the scan orbit does not accurately outline the body boundary, it will constrain the dotted lines to drop to zero close enough as one expected. The *a priori* known attenuation coefficients and the iterative process will further constrain the drop-off via the iterative MAP algorithm of Eq.(2).

The algorithms of Eqs.(2) and (3) are coded in such a way that the reconstructions have the same size as the source. So the orbit constraint is directly input to the reconstruction of the attenuation map, and the map is then directly used to reconstruct the emission data. The coding considers the symmetries of 120 projections evenly spaced over 360 degrees through a square image array. Only a half quarter of projections (from 0 to 45 degrees) are employed to compute the matrix elements $\{T_{ij}\}$ and $\{R_{ij}\}$, respectively. The computed elements are then used for the rest projections because of the symmetries. And so the computing time is significantly reduced.

III. RESULTS

A chest phantom of 128^2 size was computer simulated. From the phantom, the corresponding attenuation map was generated. A fan-beam projector was used to simulate the transmission data at 120 projection angles uniformly distributed over 360 degrees from the attenuation map. A parallel-beam projector was applied to synthesize the emission scans using the chest phantom and its attenuation map. The fan- and parallel-beam projectors and backprojectors were coded using the ray-tracing method [29], so the projection-transform matrix T_{ij} represents the intersecting length of ray i within voxel j. The matrix R_{ij} is the product of T_{ij} and the corresponding attenuation factor along ray i from voxel j to the collimator [1]. A set of completely-sampled transmission data was first simulated. The truncated data were then generated by limiting the field-of-view (FOV) of the fan-beam collimator. More than half of the 120 projections were truncated due to the limited FOV. In order to show the truncation effect, there is no noise imposed on the simulated data.

For comparison, the completely-sampled data set of fan-beam geometry was first reconstructed. The FBP recon-

[14] E. Frey, Z. Ju and B. Tsui, "A Fast Projector/Backprojector Pair Modeling the Nonstationary Scatter Response Function for Scatter Compensation in SPECT Imaging," Proc. IEEE TMI, vol.2, pp.1032-1034, 1992

[15] Z. Liang, "An Efficient 3D Unified Projector-Backprojector for SPECT Reconstruction," Proc. IEEE TMI, vol.3, pp.1975-1979, 1991

[16] K. Ogawa, A. Chugo, T. Ichihara, A. Kubo and S. Hashimoto, "Quantitative Image Reconstruction Using Positon-Dependent Scatter Correction in SPECT," Proc. IEEE TMI, vol.2, pp.1011-1013, 1992

[17] Z. Liang and J. Ye, "Quantitative SPECT Using Cone-Beam Collimation and Iterative FBP Reconstruction," Proc. World Chinese Nuclear Medicine Society, 1993

[18] M. King, G. Hademenos and S. Glick, "A Dual Photo-Peak Window Method for Scatter Correction," JNM, vol.33, pp.605-612, 1992

[19] K. Ogawa, Y. Harata, T. Ichihara, A. Kubo and S. Hashimoto, "A Practical Method for Position-Dependent Computon-Scatter Correction in SPECT," IEEE TMI, vo.10, pp.408-412, 1991

[20] C. Pierno, D. Band and S. Lorber, "Tc-99m Transmission-Emission Scanning," JNM, vol.12, pp.481, 1971

[21] D. Bailey, B. Hutton and P. Walker, "Improved SPECT Using Simultaneous Emission and Transmission Tomography," JNM, vol.28, pp.844-851, 1987

[22] B. Hasegawa, E. Gingold, S. Reilly, S. Liew and C. Cann, "Description of a Simultaneous Emission-Transmission CT System," SPIE Med Imaging IV, vol.1231, pp.50-60, 1990

[23] S. Manglos, D. Bassano, C. Dexbury and R. Capone, "Attenuation Maps for SPECT Determined Using Cone-Beam Transmission Computed Tomography," IEEE TNS, vol.37, pp.600-608, 1990

[24] D. Gilland, R. Jaszczak, T. Turkington, K. Gree and E. Coleman, "Quantative SPECT Imaging with Indium-111," IEEE TNS, vol.38, pp.761-766, 1991

[25] C. Tung, G. Gullberg, G. Zeng, P. Christian, F. Datz and N. Morgan, "Non-Uniform Attenuation Correction Using Simultaneous Transmission and Emission Converging Tomography," IEEE TNS, vol.39, pp.1134-1143, 1992

[26] R. Jaszczak, D. Gilland, S. Jang, K. Greer and E. Coleman, "Fast Transmission CT for Determining Attenuation Maps Using a Collimated, Shattered Line Source and Fan-Beam Collimation," Proc. IEEE TMI, vol.2, pp.991-993, 1992

[27] Z. Liang, R. Jaszczak, E. Coleman and V. Johnson, "Simultaneous Reconstruction, Segmentation, and Edge Enhancement of Relatively Piecewise Continuous Images with Intensity-Level Information," Med. Physics, vol.18, pp.394-401, 1991

[28] Z. Liang, R. Jaszczak and E. Coleman, "On Reconstruction and Segmentation of Piecewise Continuous Images," Proc. IPMI, vol.12, pp.94-104, 1991

[29] R. Siddon, "Fast Calculation of the Exact Radiological Path for a 3D CT Array," Med. Physics, vol.12, pp.252-255, 1985

[30] K. Lange and R. Carson, "EM Reconstruction Algorithms for Emission and Transmission Tomography," JCAT, vol.8, pp.306-316, 1984

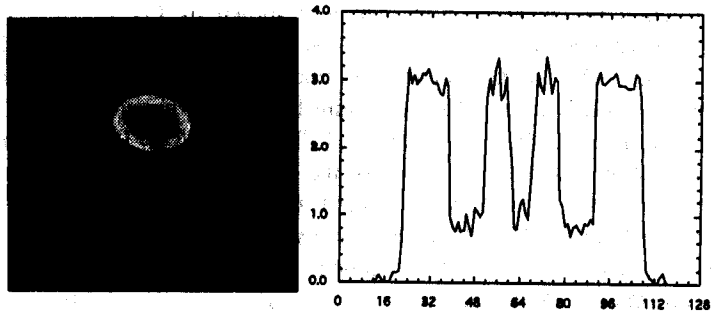

Fig.1: The reconstruction of a thorax phantom from 128 cone-beam collimated projections of 128^2 size. The cross-sectional image is one-slice off the central plan of a 128^3 array. The one-pixel-wide profile is drawn horizontally through the center of spinal bone.

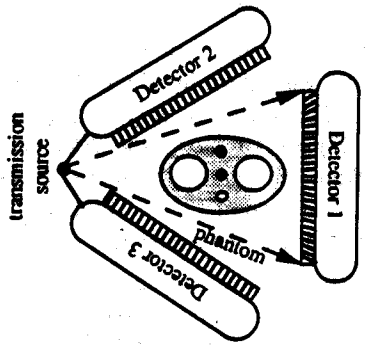

Fig.2: The configuration for an external line-source transmission scan using a three-headed SPECT system.

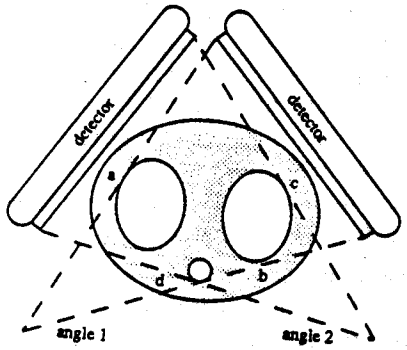

Fig.3: A diagram describing the truncation of a fan-beam collimation.

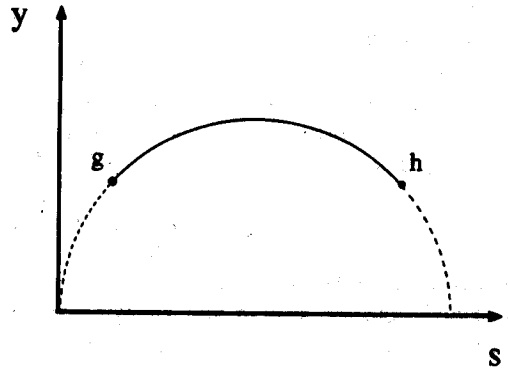

Fig.4: The continuity constraint at positions g and h for the reprojected data from truncated areas (as shown by the dotted lines) and the measured data (as shown by the solid line).

struction of the atenuation map was shown by Fig.5. The fan-beam geometric weight was considered in the backprojection. The parallel-beam collimated projections were reconstructed using the maximum-likelihood expectation-maximization (ML-EM) algorithm [30] (i.e., set $N_k = 0$). Figure 6 shows the reconstruction of the chest phantom from the parallel-beam projections with the true attenuation map after 20 iterations. If the attenuation map was not used, the reconstruction was significantly degraded, as shown by Fig.7. If a uniform attenuation map was used, the reconstruction did not have any improvement as demonstrated in Fig.8. The object-specific attenuation map is very necessary. The nonuniformity in the reconstructions across the uniform-intensity regions is due to the partial-volume effect associated with the model in computing T_{ij} and R_{ij}.

The FBP reconstruction of the attenuation map from the truncated data was shown by Fig.9. The truncation effect is clearly seen. The effect is very damaging to emission reconstruction. Figure 10 shows the 20th iterated ML-EM reconstruction from the parallel-beam projections using the truncated attenuation map of Fig.9. The intensity at the truncated areas is much lower than expected.

The reconstruction using the MAP-EM algorithm of Eq.(2) from the truncated transmission data is shown by Fig.11 after 20 iterations. The initial estimate was the FBP reconstruction of Fig.9. The truncation effect was significantly reduced by the simultaneous reconstruction and segmentation of different regions of bone, lungs, and soft tissues. The algorithm was completely data driven without any freely adjustable parameter. Using the compensated attenuation map of Fig.11, the 20th iterated ML-EM reconstruction from the emission data is shown by Fig.12. The reconstruction using the MAP-EM algorithm of Eq.(3) is similar to that of Fig.12, except that the MAP result is smoother within the regions of bone, lungs, and soft tissues.

The reconstruction time for the ML-EM and MAP-EM of Eq.(3) algorithms were similar and was less than 5 minutes on a HP/730 desktop computer. The reconstruction of Fig.11 from the truncated transmission data took less than 2 minutes.

The error of reconstructed intensities over the region of soft tissues was 11% between the results of Fig.10 and Fig.6. While the error between Fig.12 and Fig.6 was 2%. It is clear that significant improvement in quantification of SPECT was achieved with the compensated attenuation map of Fig.11, as compared to the reconstruction using the truncated attenuation map of Fig.9.

IV. CONCLUSION

A method for quantitative SPECT reconstruction using a three-headed detector system and an external radioactive line source was described. The truncation effect associated with the fan-beam geometry was compensated by a MAP approach which simultaneously reconstructs and segments the object-specific attenuation map. The *a priori* known attenuation coefficients of bone, lungs, soft tissues, and air were incorporated into a Bayesian framework. The continuity constraint for reprojection was described, and the scan orbit was used to estimate the initial ranges of the reprojections. From the compensated attenuation map, the accuracy of quantitative reconstruction of emission data was significantly improved.

V. REFERENCES

[1] Z. Liang, "Compensation for Attenuation, Scatter, and Detector Response in SPECT Reconstruction via Iterative FBP Methods," Med. Physics, vol.40, pp.1097-1106, 1993

[2] G. Zeng and G. Gullberg, "Frequency Domain Implementation of the 3D Geometric Point Response Correction in SPECT Imaging," IEEE TNS, vol.39, pp.1444-1453, 1992

[3] S. Glick, B. Penney, M. King and C. Byrne, "Non-Iterative Compensation for the Distance-Dependent Detector Response and Photon Attenuation in SPECT Imaging," Proc. IEEE TMI, vol.2, pp.1172-1174, 1992

[4] N. Rajeevan, B. Penney and M. King, "Quantitative SPECT Imaging: Compensation for Nonuniform Attenuation, Scatter, and Detector Divergence," Proc. IEEE TMI, vol.2, pp.995-997, 1992

[5] Z. Liang, T. Turkington, D. Gilland, R. Jaszczak and E. Coleman, "Simultaneous Compensation for Attenuation, Scatter, and Detector Response for SPECT Reconstruction in Three Dimensions," Phys. Med. Biol., vol.37, pp.587-603, 1992

[6] G. Zeng, G. Gullberg, B. Tsui and J. Terry, "Three Dimensional Iterative Reconstruction Algorithms with Attenuation and Geometric Point Response Correction," IEEE TNS, vol.38, pp.693-702, 1991

[7] A. Formiconi, A. Passeri, A. Pupi and G. Comis, "High Resolution Brain SPECT with Accurate Modeling of Spatial System Response, Attenuation and Scatter," JNM, vol.31, pp.739, 1990

[8] B. Tsui, G. Gullberg, E. Edgerton, J. Ballard, et al, "Correction of Nonuniform Attenuation in Cardiac SPECT Imaging," JNM, vol.30, pp.497-507, 1989

[9] C. Floyd, R. Jaszczak, K. Greer and E. Coleman, "Inverse Monte Carlo as a Unified Reconstruction Algorithm for ECT," JNM, vol.27, pp.1577-1585, 1986

[10] R. Jaszczak, K. Greer, C. Floyd, C. Harris and E. Coleman, "Improved SPECT Quantification Using Compensation for Scattered Photons," JNM, vol.25, pp.893-900, 1984

[11] Z. Liang, R. Jaszczak, C. Floyd, K. Greer and E. Coleman, "Reprojection and Backprojection in SPECT Image Reconstruction," Proc. IEEE Energy Inform. Tech. Southeast, vol.1, pp.919-926, 1989

[12] R. Huesman, G. Gullberg, W. Greenberg and T. Budinger, *Donner Algorithms for Reconstruction Tomography* (Lawrence Berkeley Laboratory, University of California, 1977)

[13] Z. Liang, R. Jaszczak, C. Floyd, K. Greer and E. Coleman, "Bayesian Reconstruction of SPECT in Parallel, Fan, and Cone Beam Geometries," JNM, vol.29, pp.871, 1988

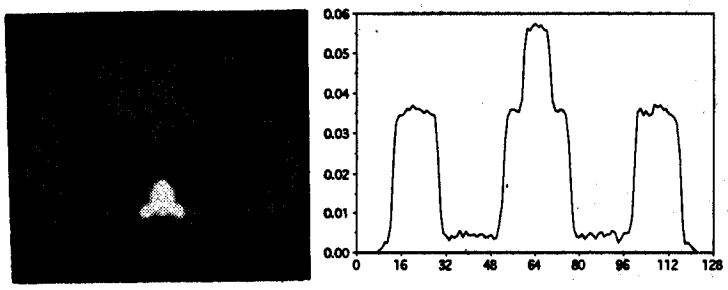

Fig.5: The reconstructed attenuation map from completely-sampled fan-beam data using FBP algorithm and its one-pixel-wide profile drawn through the center of spinal bone horizontally.

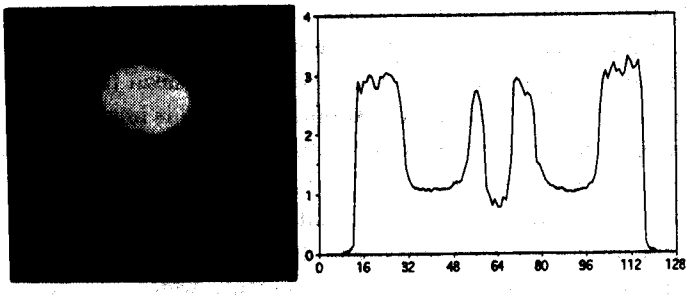

Fig.6: The reconstructed emission image using the true attenuation map and parallel-beam data by the ML-EM algorithm after 20 iterations and its horizontal profile through the center of spinal bone.

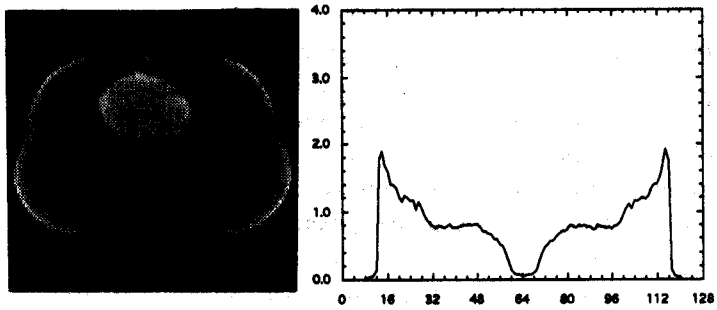

Fig.7: The emission reconstruction without attenuation compensation using the ML-EM algorithm after 20 iterations and its horizontal profile through the center of spinal bone.

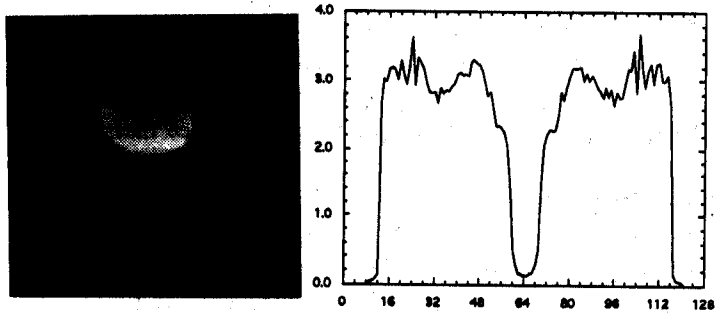

Fig.8: The emission reconstruction using a uniform attenuation map by the ML-EM algorithm after 20 iterations and its horizontal profile through the center of spinal bone.

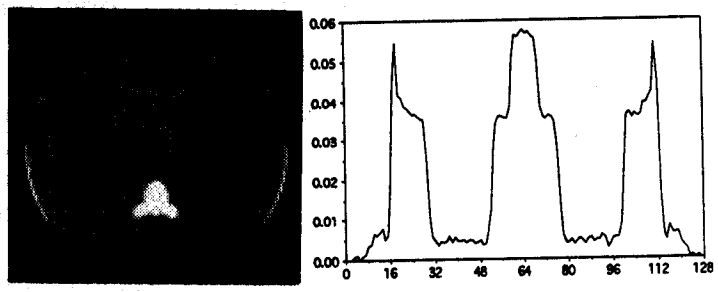

Fig.9: The reconstructed attenuation map from the truncated fan-beam transmission data using FBP algorithm and its horizontal profile through the center of spinal bone.

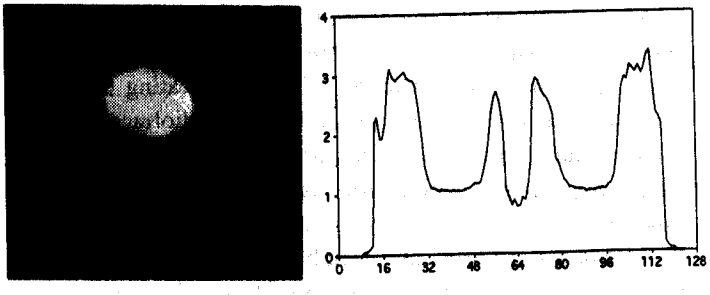

Fig.10: The reconstructed emission image using the truncated attenuation map of Fig.9 by the ML-EM algorithm after 20 iterations and its horizontal profile through the center of spinal bone.

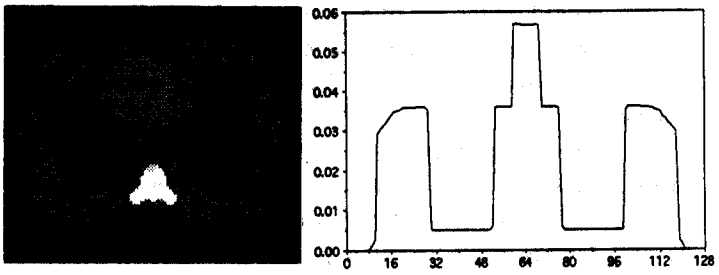

Fig.11: The reconstructed attenuation map from the truncated fan-beam data using the MAP-EM algorithm of Eq.(2) after 20 iterations and its horizontal profile through the center of spinal bone.

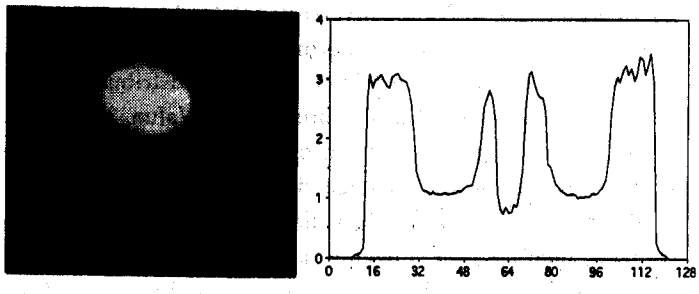

Fig.12: The reconstructed emission image using the compensated attenuation map of Fig.11 by the ML-EM algorithm after 20 iterations and its horizontal profile through the center of spinal bone.